

Perovskite Solar Cells with Vivid, Angle-Invariant, and Customizable Inkjet-Printed Colorization for Building-Integrated Photovoltaics

Helge Eggers,* Saba Gharibzadeh, Stefan Koch, Fabian Schackmar, David B. Ritzer, Tobias Abzieher, Bryce S. Richards, Christof Erban, and Ulrich W. Paetzold*

The steadily growing market share of building-integrated photovoltaics (BIPVs) places the aesthetics of solar modules in the focus of research and development. In this work, a colorization method based on inkjet-printed reflective pigments is adapted for the emerging perovskite photovoltaics. Herein, not only excellent control of color impression, brightness, and pattern is demonstrated, but also angle invariant color perception, which makes the presented approach stand out among the many published colorization strategies for perovskite solar cells (PSCs). Compared to uncolored reference solar cells, bright magenta and yellow PSCs display a remarkable relative power conversion efficiency (PCE) of up to 65% and more than 11% absolute PCE. Moreover, PSCs with more BIPV-relevant coloring patterns such as a mimic of a marble or corten steel surfaces are demonstrated. The colorization method presented is inexpensive and ready for scalable solar module production. To demonstrate the scalability of the proposed concept, a small-area perovskite solar module (4 cm² aperture area) in white marble optics exhibiting a PCE of almost 14% as a potential application is presented.

1. Introduction

The steadily increasing demand for renewable electrical energy, particularly in regions with high population density, entails a growth of the market for building-integrated photovoltaics (BIPVs) with up to 40% annual growth rates being predicted over the next decade.^[1,2] These outlooks are founded on conventional solar cell technologies, however, next generations of photovoltaic (PV) technologies—such as perovskite solar cells (PSCs)—could add further benefits for BIPV: First, the overall high power conversion efficiency (PCE) achieved for PSCs of up to 25.7%^[3] is not only promising in itself, but also serves to pay the way for perovskite-silicon tandem solar cells that exhibit even higher PCEs. Even today, the record PCEs of 29.5%^[3] for such tandem devices is well

above the record for single-junction crystalline silicon solar cells on the laboratory scale. Second, PSCs offer the ease of facile processing from solution as well as evaporation-based fabrication processes. Recent advances in blade-coating,^[4,5] inkjet printing,^[6,7] and thermal evaporation^[8,9] bring fast and scalable industrial fabrication into reach. Third, perovskite PV, as a solution-processable thin-film technology, offers easily achievable freedom in design in shape^[7] and transparency^[10,11] by thickness- and form-controlled film deposition via printing technologies.

Of key importance for the economic widespread and market acceptance of photovoltaics in buildings is aesthetics, in particular its color appearance.^[12–15] The additional costs for such customized BIPV solar modules vary in a vast range depending not only on the underlying study layout but also on the factors as the targeted geographical region and the system's design.^[16] Following estimations, the cost offset of BIPV materials compared to traditional construction materials ranges from 5000% for replacing concrete roofs tiles^[17] to 80% when replacing polished stone facades.^[18] These findings indicate that in the case of expensive building materials such as polished stone, which are applied where there are high demands on the aesthetic of the building, BIPV components might be a possible alternative building materials—provided that these can also fulfill the product demands. For conventional PV technologies such as silicon, a broad spectrum of different design options has been investigated

H. Eggers, S. Gharibzadeh, F. Schackmar, D. B. Ritzer, T. Abzieher, B. S. Richards, U. W. Paetzold
Karlsruhe Institute of Technology
Light Technology Institute (LTI)
76131 Karlsruhe, Germany
E-mail: helge.eggers@kit.edu; ulrich.paetzold@kit.edu

H. Eggers, F. Schackmar
InnovationLab
69115 Heidelberg, Germany

H. Eggers, S. Gharibzadeh, F. Schackmar, D. B. Ritzer, B. S. Richards, U. W. Paetzold
Karlsruhe Institute of Technology
Institute of Microstructure Technology (IMT)
76344 Eggenstein-Leopoldshafen, Germany

S. Koch, C. Erban
SUNOVATION Produktion GmbH
63820 Elsenfeld, Germany

 The ORCID identification number(s) for the author(s) of this article can be found under <https://doi.org/10.1002/solr.202100897>.

© 2022 The Authors. Solar RRL published by Wiley-VCH GmbH. This is an open access article under the terms of the Creative Commons Attribution-NonCommercial License, which permits use, distribution and reproduction in any medium, provided the original work is properly cited and is not used for commercial purposes.

DOI: 10.1002/solr.202100897

and evaluated.^[14] In recent years, some of these concepts, as well as new approaches that are more specific to the perovskite thin-film technology, have been proposed to realize both colorful semitransparent^[19–26] and opaque^[27–35] PSCs. It is, for example, possible to vary the color of the perovskite absorber layer itself by changing its chemical composition, thus altering its crystal structure and bandgap. However, such alteration of the absorber material itself implies compromises on the harvested part of the solar spectrum and further changes of the chemical and optoelectric properties like the (temperature) stability.^[35] To retain these properties and the benefit from the economics-of-scales that optimized fabrication processes for non-colored PSCs may provide, colorizations using interference effects of thin films in the solar cell stack such as transparent electrodes,^[19,22,25,29,31] charge extraction layers,^[28] or additional layers^[23,32,34] have advanced to promising strategies. Many of these strategies have been adapted from research on colorful conventional photovoltaics.^[14,36] In case of colorful PSCs, the work of Jiang et al. merits to be mentioned as they reach high PCEs of 11.6% (red) to 13.8% (blue) for a variety of colored PSCs by the integration of transparent top polymer electrodes of different thicknesses.^[29] Recently, Yoo et al. proved that these efficiencies could be enhanced even further. By the addition of nonperiodic multi-nanolayer, narrow-bandwidth-reflective filters to their PSCs, they achieved PCEs of 18.0%, 18.6%, and 18.9% for red, green, and blue devices respectively,^[34] exceeding the theoretical efficiency limit of ideal colored opaque solar photovoltaics.^[37] However, a tremendous disadvantage of the structural colorization as applied in this study is the reliance on interference effects, which are by nature subject to a strong dependence of the observation and incident light angle. As a consequence, for example, large facades in BIPV would risk to appear nonuniform from the perspective of an observer. While such a nonuniform and angle-dependent appearance might be desired in some cases, the authors of this work are convinced that the BIPV community would appreciate the possibility of choice of design. In response to this challenge, we present the adaptation of an industrial-proven concept of colorization by inkjet printing pigment-based reflective and transmissive layers on the solar

module's front side. In view of the high absorption coefficient and therefore dark color-impression of perovskite, white interlayers with different saturations are used as a reflector and their effect on the color-impression as well as PCE of the device is characterized. This method allows not only for bright and angle-independent colorization with continuously adjustable lightness, but also for freedom in the design pattern. The colorization is independent of the solar cell architecture and, as a single-step inkjet printing process, promises to be simple and consequently cost-effective to realize. Compared to uncolored reference devices' relative PCEs of 65% to 70% and maximum absolute PCEs of more than 10% to 12% can be achieved for bright mono-colored magenta or, respectively, yellow PSCs. To indicate the adaptability of this process toward actual applications in BIPV, we fabricated a small module prototype in a marble optic that displays almost 14% PCE. In a nutshell, this work suggests that the presented approach might be suitable for the colorization of PSCs with high aesthetic demands.

2. Colorization of PSCs

The presented method to colorize PSCs is based on inkjet-printed colored glass substrates. Colorization via this approach was pioneered for crystalline silicon photovoltaics and is available today on the PV market.^[38] Here, we adapt this concept for perovskite photovoltaics: In this study, the pigment-based colored layers are inkjet-printed on the plain glass side of pre-patterned indium tin oxide (ITO) glass substrates. Subsequently, the PSC layer stack is deposited on the ITO side of the substrate (Figure 1a). This approach of colorization is, with regards to fabrication, mostly independent on the solar cell architecture. PSCs with both nip- and pin-architecture were fabricated and used for relative and absolute comparison of the performance of the colored PSCs (see Section 3). In this work, all devices are characterized without additional encapsulation to facilitate characterization. Although the colored layers display very high stability to mechanical and light-induced stress (see Figure S1, Supporting Information), for commercial application an additional encapsulation is intended. This has already proven

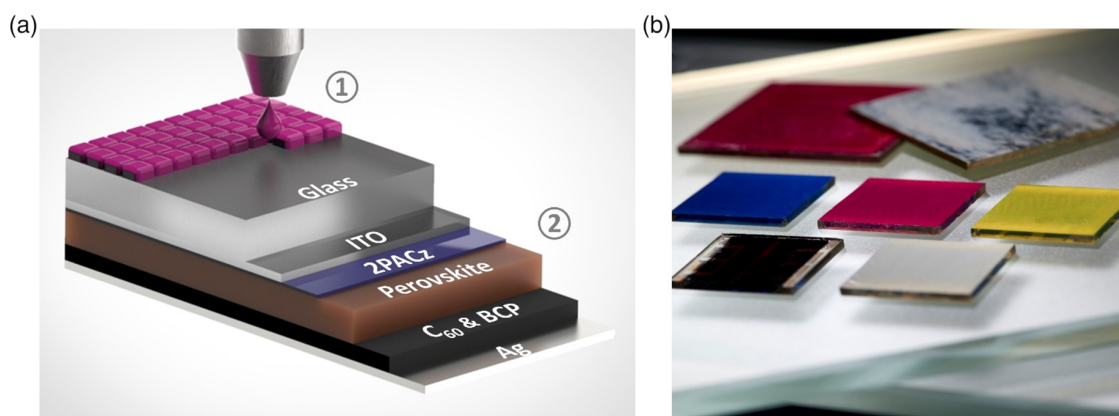


Figure 1. a) Schematic of the colored perovskite solar cell with the pigment-based colored layers inkjet-printed on the front side of the glass substrate first (1) and the different solar cell layers (here of pin-architecture) deposited on the rear side afterward (2). b) Photograph of PSCs and modules colorized with inkjet-printed pigments in various bright colors and color patterns.

applicable for commercially available colorful crystalline silicon following a similar colorization approach^[38] and would be transferable to PSCs given the multitude of possible encapsulation methods that are under investigation.^[39] To illustrate the vivid and versatile colorization that is possible with the presented approach, in addition to the primary colors of the subtractive (cyan, magenta, yellow) and additive (red, blue, green) color schemes, complex color patterns were printed on the glasses to imitate popular construction materials such as marble or rusted steel, so-called corten steel (Figure 1b). While multicolored patterned perovskite photovoltaic were realized before by large pixels^[29] or randomized reflection structures^[27] such customizable and refined colorization is unprecedented and beyond what is possible to achieve by so far reported colorization methods based on structural colorization.

In a first step, single layer colorization of PSCs is evaluated. We use four different pigment-based inks of white, cyan, magenta, and yellow color. The mean thickness of the layer is controlled by the printing saturation which is a printer-specific parameter (see Experimental Section) and can be directly correlated to the optical properties of transmittance and reflectivity (Figure S2, S3, Supporting Information). Here, the colored layers' transmittance and color impression in front of a white and dark background are investigated for different saturations. Although a bright color impression can be easily achieved on white background for a variety of colored substrates, for many of these the targeted color impression cannot be achieved on dark background even for increasing printing saturations up to 100% (Figure S4, Supporting Information). Instead, the printed glasses' color generally lack brightness, respectively, the corresponding lightness L^* in the CIELAB color system is used for characterization here (compare Experimental Section). To increase the lightness and obtain a color impression as close as possible to the targeted color, a reflective interlayer between the PSC and the printed pigment film is introduced. To maintain the simplicity of the process, a layer of white pigment deposited by inkjet printing is chosen. With the saturation of the white interlayer, the solar cell's reflectivity, therefore the lightness, and with it, the overall color of the PSC can be tuned and bright color impressions can be achieved (Figure 2a). Figure 2b displays the color impression of PSCs in cyan, magenta, and yellow with fixed saturation on top of varying interlayer saturations in a conventional 2D CIE1931 xy -diagram. Additionally, targeted color impressions of colored glasses without any additional layers on the white background are visualized by their color coordinates. Since the differences in the lightness cannot be represented in the 2D diagram and differences in color are not uniformly displayed in CIE1931, the projections of a 3D CIELAB diagram are provided as an additional visualization method (Figure 2c). Here, the measured colors are represented by their unique position in the CIELAB color space (compare Figure S5 and Table S6, Supporting Information) and, to some extent, by the marker colored in corresponding RGB-values. In particular, the projections of the 3D representation show that the color impression of the PSCs with white interlayer is very close to the targeted color on a white background and significantly more brilliant and colorful than without the white interlayer.

Many previous publications on the colorization of PSCs are based on structural interference of parts of the incoming and

partially reflected light in or between various thin layers of the device.^[19,22,23,25,28,29,31] These approaches offer a high reflectivity for the narrow color-defining spectral range and therefore maximize light harvesting in the colored PSCs. However, structural interference generally leads to a strong angle dependence of the generated color. Recent work by Bläsi et al. suggests that this angular dependency might be bypassed even for interference-based colorization.^[40] So far, in the majority of publications on colored PSCs,^[19–21,21,22,24–34] the dependency of the color impression on both the viewing angle and the incident angle of the light is insufficiently characterized. Whenever this angular dependency is discussed, the color impression is found to vary for viewing angles $>20^\circ$ – 30° .^[28,34] Even colorful semi-transparent PSCs that are intended to serve for color-invariant applications show shifts in peak transmission, and therefore alteration of the color impression, for different incident angles starting at $>40^\circ$ – 60° depending on the intended color.^[25] While some research groups claim that such an angular dependent color impression might increase the aesthetic value,^[24,34] we are convinced that for many applications vivid yet angle-independent perovskite solar cell colorization is desired. As such, the pigment-based colorization method presented here is angle-invariant. The reason is that it is not based on structural interference between different layers of the device but rather on the selective reflection of light at ink's pigment particles. As displayed in Figure 3, for the given detection sensitivity, the color impression of the colorized PSCs is in first-order independent of the viewing angle even for large incident angles of at least 70° . This angle-invariant color impression is a key advantage over other colorization methods for many applications in BIPV, such as large façades that would appear multicolored depending on the observer's point of view and wherever the customer has a specific demand on the color impression, an example given for corporate designs.

3. Performance of Colorful PSCs

Compared to silicon solar cells, the absorption spectrum of perovskite is generally shifted to shorter wavelengths and consequently toward the visible part of the spectrum. As a consequence of the colorization by selectively transmissive pigment layers, the performance of the solar cell is impacted even more – especially if combined with a reflective white interlayer. In a first step, the reflective white interlayer is analyzed to obtain a compromise between maximum performance without any white interlayer and the brightest color impression using a thick white interlayer. To achieve maximal reproducibility of the color impression, the first set of printed pigment inks covers the primary colors such as cyan, magenta, and yellow. Each color is printed with a saturation of 100% on ITO-glasses with white layers of 60%, 80%, and 100% saturation on the front side as well as on a reference glass without any white interlayer (0%). These colorized glasses are used to process the functional layers of PSC on the ITO-sputtered rear side of the glass (see Figure 1a), both, in nip- and pin-double-cation perovskite solar cell architectures. Details on the layer stacks as well as fabrication methods are specified in the Experimental Section. The performance of the solar cells is evaluated under illumination with a solar simulator AM1.5G-solar

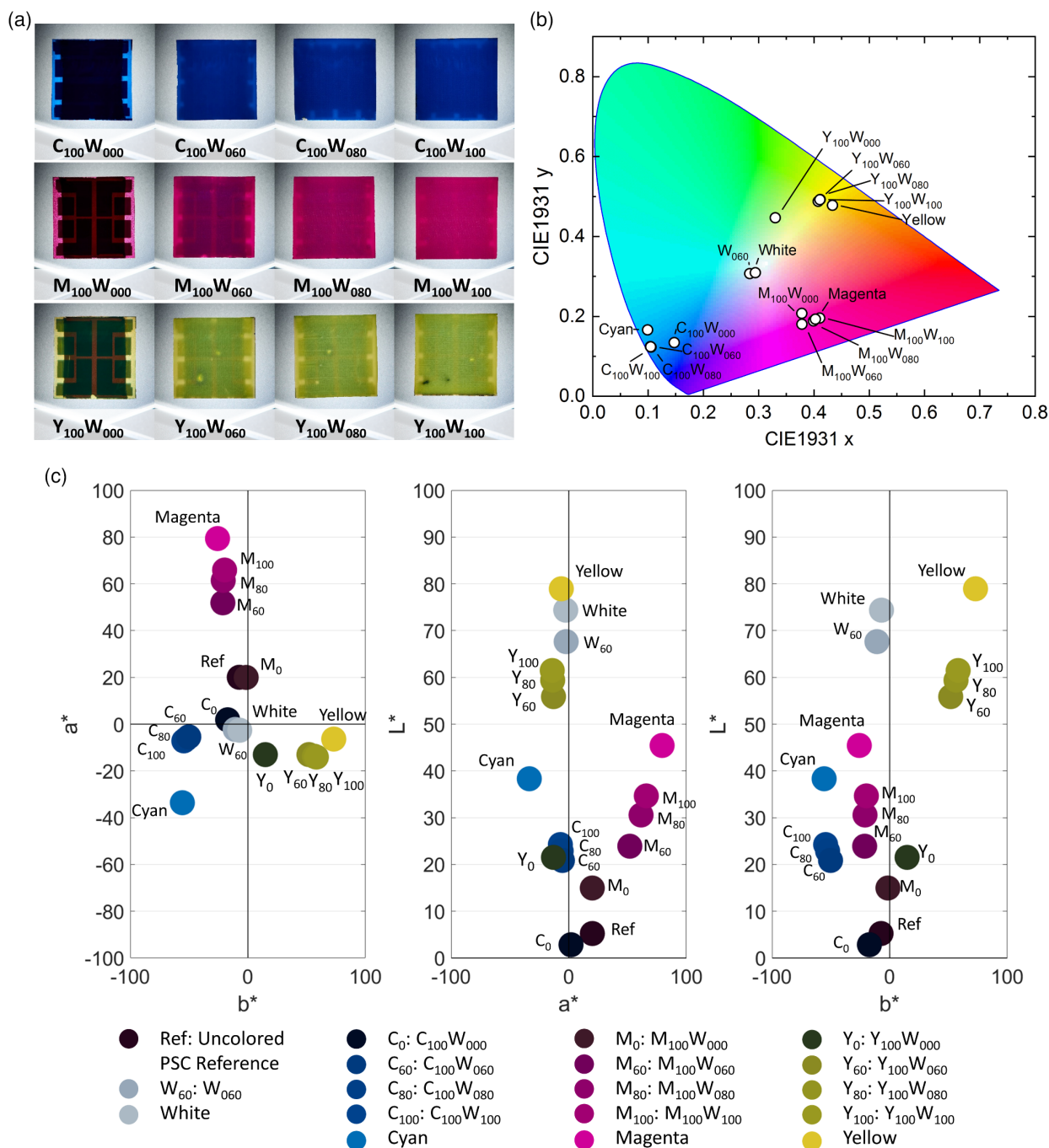


Figure 2. a) Photographs of colorful PSCs fabricated by the described process. The saturation of the white interlayer is increased from 0% (no interlayer) over 60% and 80% to 100% from left to right. b) Characterization of the color impression of the PSCs in a conventional 2D CIE1931 presentation: Color impression of PSCs in white (W) as well as cyan (C), magenta (M), and yellow (Y) with a fixed printing saturation of 100% and varying saturations of x% of the white interlayer W_x are shown. As a reference, the intended color impression of colored glass on a white background is displayed (“White”, “Cyan”, “Magenta”, “Yellow”). c) Characterization of the same PSCs as represented before in projections of the 3D CIELAB color space. The color of each data point represents the measured color impression converted to RGB values.

spectrum. To exclude the possibility of increased illumination through repeated reflection between the colored substrate surface and solar simulator lens, two different setups with differing beam paths and beam path lengths have been utilized. Even

for strong reflective white PSCs, the PCE agrees within the given measurement sensitivity and statistic deviations (Figure S7, Supporting Information), suggesting that there is no underlying systematic overestimation.

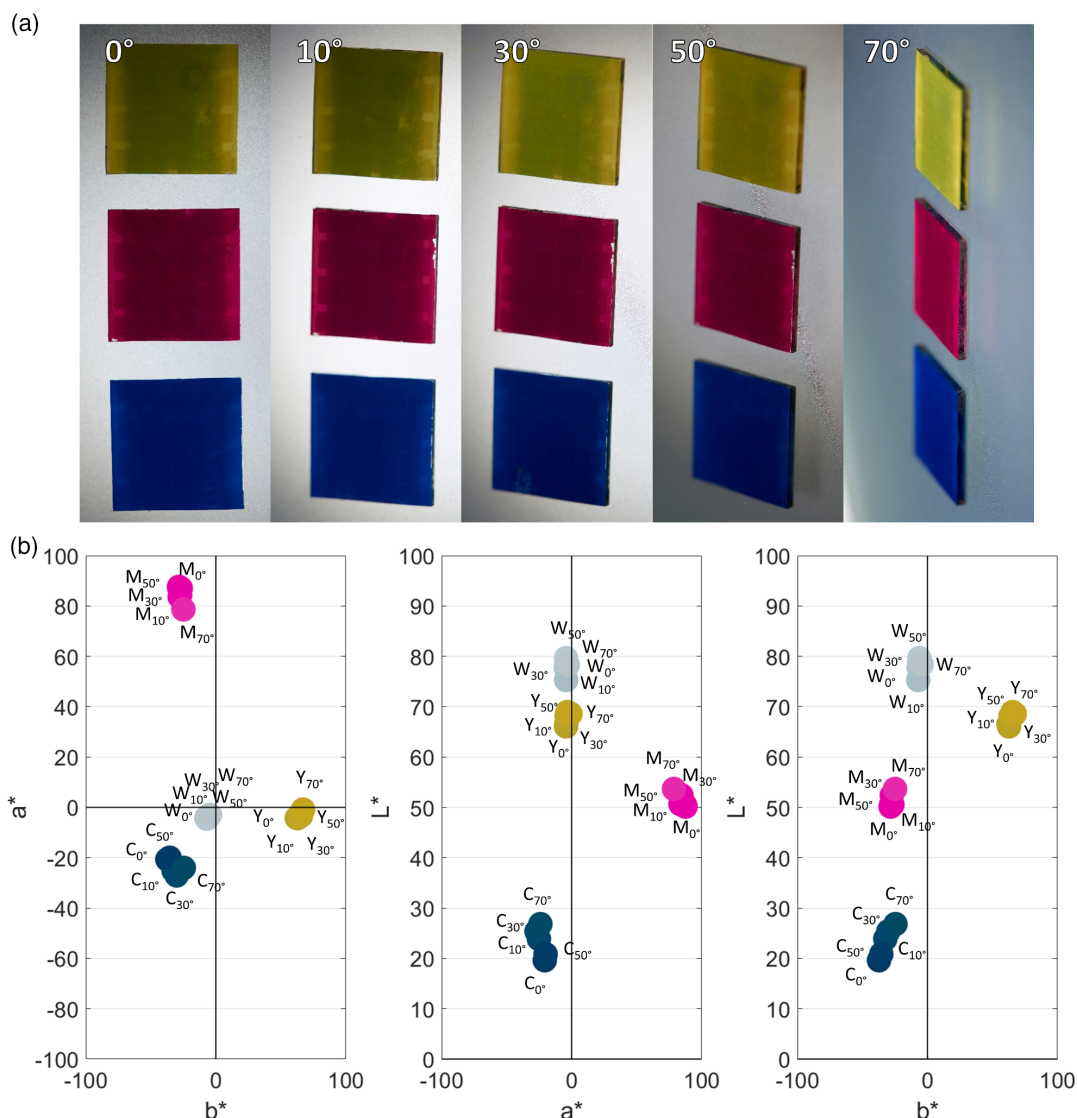


Figure 3. a) Photographs of colorful PSCs under different viewing angles (0°–70°). b) Characterization of the color impression of the colorful PSCs (cyan (C), magenta (M), yellow (Y), and white (W)) under different viewing angles (0°–70°) in projections of a customized 3D CIELAB presentation. Color values were measured under illumination with a non-standardized light source and normalized afterward (see Experimental Section). The color of each data point represents the measured and normalized color impression converted to RGB values. The shift in the color impression is hardly distinguishable in the given measurement sensitivity.

Overall the same trends for the interplay between colorization and PSC performance are apparent for nip- and pin-architectures for all colors investigated (Figure 4a,b): For single layers of magenta and yellow relatively low losses in performance of around 10–30% are apparent compared to the uncolored reference, whereas cyan-colored devices suffer from 50% to 70% PCE loss. These differences originate from the significantly differing parts of the solar spectrum that are reflected and therefore lost for photo-absorption in the perovskite (Figure 4c). As expected the PCE decreases with implementation and augmentation of saturation of the white interlayer for all printed colors. In comparison to the results of the aforementioned color evaluation, a

white interlayer of 60% saturation is sufficient to achieve vivid colorization. PSCs colored with only the white interlayer maintain on average 70–80% of the initial PCE, which is a remarkable high value for whitish solar cells. Printing the white pigment as an interlayer on top of the glass before printing the intended colors increases the brightness of the color significantly but on average still maintains good relative PCEs of up to 65% to 70% for magenta or yellow. Best performing PSCs with such a white interlayer display an absolute PCE of 3.3%, 10.2, and 12.4% for bright cyan, magenta, and yellow colorization, respectively (Figure 4d) in both current–voltage scan and maximum power point measurements (see Figure S8, Supporting Information).

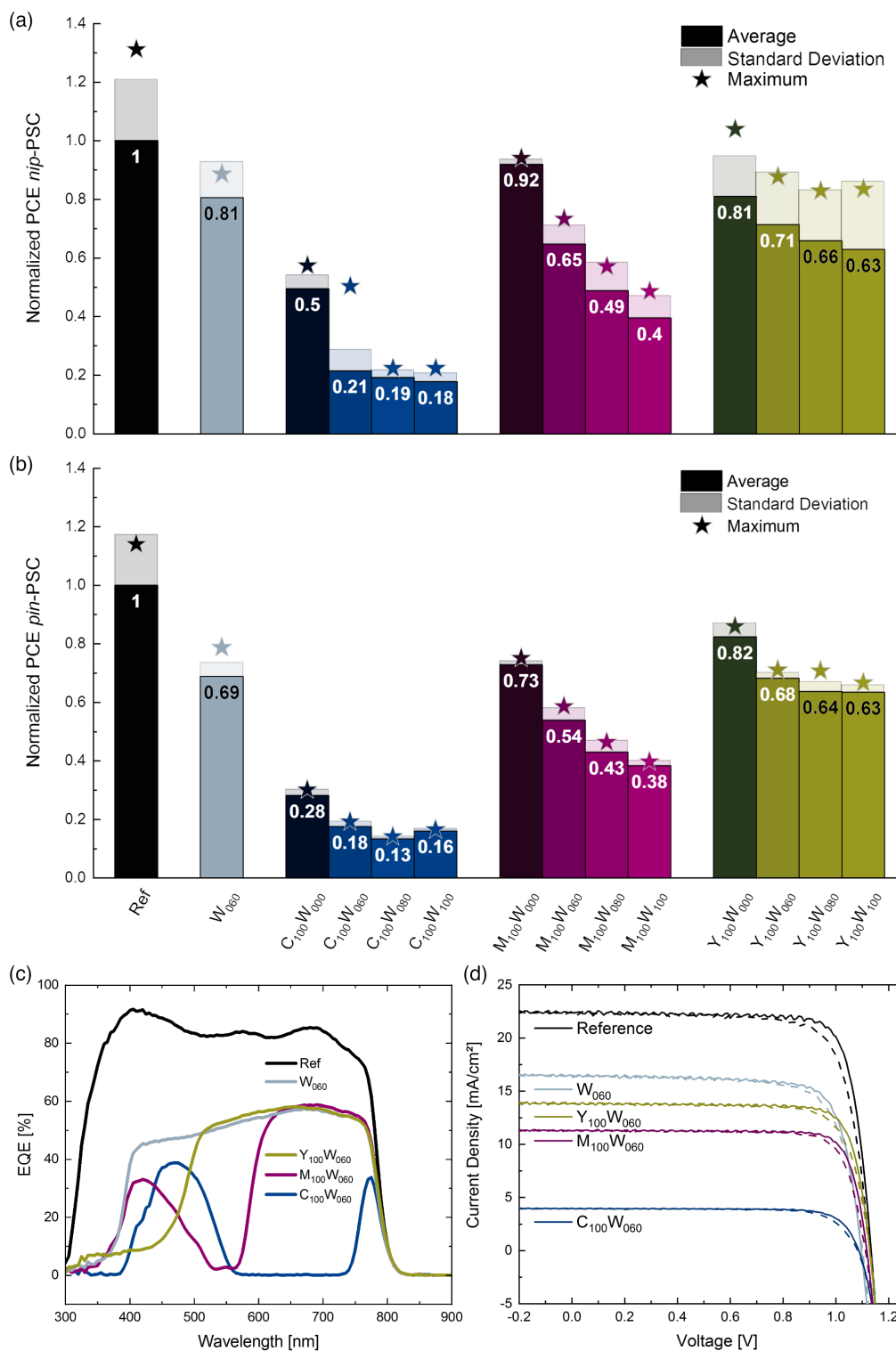


Figure 4. a) Normalized PCE of PSCs in *nip*-architecture with pigments of cyan (C), magenta (M), yellow (Y), and white (W) printed with a saturation of 100% and varying saturations $x\%$ of white interlayer W_x . For each color, the average over backward and forward current–voltage measurements of all corresponding PSCs are displayed normalized to the average of the reference cells (Ref) without color. In addition, the 1σ -standard deviation (semi-transparent column) and maximum PCE (stars) are shown. The columns are colored in the PSCs' measured color impression, converted to RGB values. b) Same data as in a) for PSCs in *pin*-architecture. c) Current–voltage scans for best performing reference, white, as well as cyan, magenta, and yellow (each with white interlayer fixed at 60% saturation) *pin*-devices in forward (dashed) and backward (solid) scan direction. d) EQE measured for white, as well as cyan, magenta, and yellow (each with white interlayer fixed at 60% saturation) PSCs in *pin*-architecture.

White-colored PSC (single-layer of 60% saturation) maintains a PCE of up to 13.7% (compare Table S9, Supporting Information).

Interestingly, an in-depth analysis of the effect of colored pigments on the solar cell performance reveals small differences for the investigated devices of the two architectures: In general, we observe a smaller loss of PCE or the PSC in nip-architecture for all colors but especially for magenta than for PSC in pin-architecture. A possible explanation would be the reduced light intensity, due to absorption and reflection of the pigments, absorbers in the colored devices are exposed too. Naturally, this reduced intensity leads to a significant drop in short-circuit current density (J_{SC}), which is the primary reason for the observed drop in PCE. At the same time, the reduced light intensity leads to an increased fill factor (FF) (Figure S10, Supporting Information). Hence, PSCs suffering from a low FF , due to, for example, architecture or deposition method, might display less loss in PCE when colorized by the presented approach than PSCs that yield a very high FF to begin with. The fundamental principle of colorization by nanometer-sized pigment-particles suggests that not only the color impression, but also the solar cell's performance displays no additional angle-variant dependency. Here, external quantum efficiency (EQE) measurements with adjustable incident angles are used to verify this hypothesis (Figure S11, Supporting Information). For comparison, we choose a strong scattering white PSC and an uncolored reference. For both the devices, the EQE slightly diminishes when going from 0° to 50° incident angle of the excitation light. The thereof calculated short-circuit current densities differ by circa 1 mA cm^{-2} for both samples, which is 7% for the white

and 4% for the reference PSC. These findings indicate that the light scattering printed pigment only adds a minor contribution to the angular dependency of the solar cell performance, which may also originate from the experimental setup (see Experimental Section).

4. Versatile Colorization for Application in BIPVs

So far, we limit our analyses to the colors of the basic inks, namely white, cyan, magenta, and yellow. However, the presented colorization method is capable of producing vivid color impressions over a large part of the CIELAB color space, as well as versatile colorization by printing arbitrary color patterns. To provide a prominent example, the commonly used primary colors of additive color generation red, green, and blue are used for colorization, setting the results of the presented approach of colorization in a better context to preceding works on colorful PSCs. To achieve these colors, the basic printing dye-inks were printed in a predefined ratio. Reflective white interlayers are used again to tune the brightness to obtain the desired color impression. **Figure 5a** shows the bright red, green, and blue PSCs performing at maximum PCE of 9.7%, 7.8%, and 5.5%, respectively (compare Figure S12, Supporting Information). This is with regards to red-colored PSCs close to commonly reported values for records of 10% to 11.6% (highest value for pinkish PSC) in literature,^[25,29,31,33] whereas Yoo et al. even reached 18.0% using very narrow-bandwidth reflective filters.^[34] A significant difference can be observed for blueish PSCs: Here the PCE

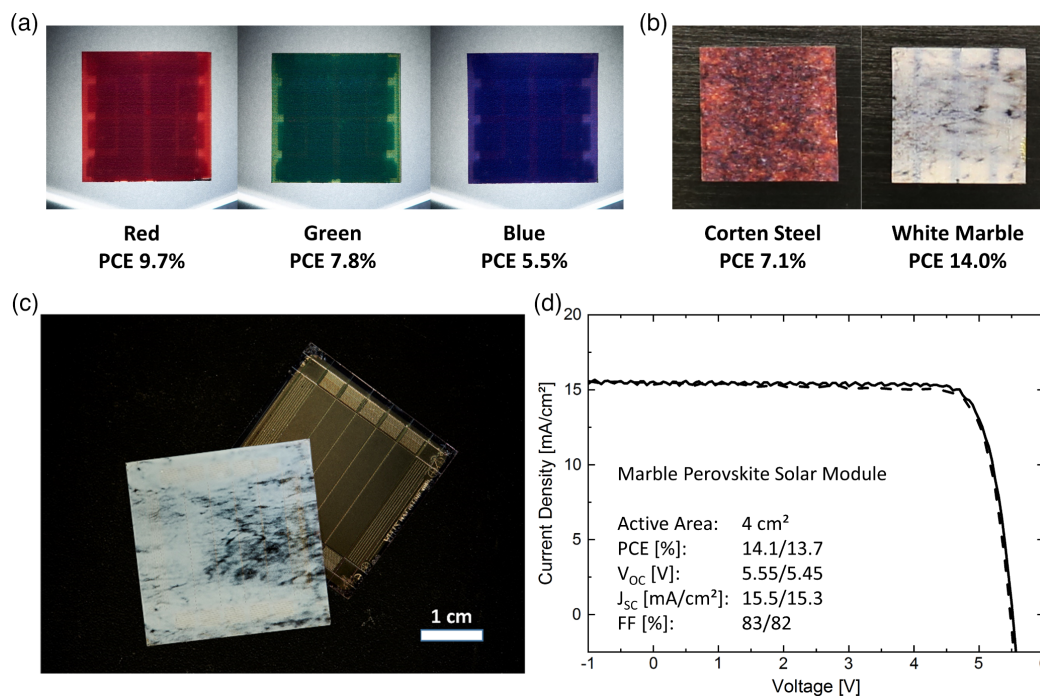


Figure 5. a) Photographs of colorful PSCs with mixed colors of red, green, and blue fabricated by the described process with average PCE of the best devices. A white interlayer of 60% saturation is incorporated into the device. b) Photographs of colorful PSCs with color patterns in corten steel and white marble optics fabricated by the described process with average PCE of the best devices. c) Photograph of a perovskite solar module in white marble optics. The size of the module is 9 cm^2 , the active area is 4 cm^2 . d) Current–voltage characteristics and photovoltaic parameters of the marble solar module shown in a).

lags significantly behind commonly reported devices in the literature with records of 13.3% to 13.8% (light blue).^[29,33] However, a detailed comparison between the different methods is hardly possible since the exact coloring (for example, the difference between magenta and red), the brightness, and exact illumination are detrimental for the measured efficiency, but not specified entirely in each publication. The presented inkjet printing colorization process allows to not only control the color, but also the coloring pattern. It is easily possible to print heterochromic patterns on basis of a digital template. As a proof-of-concept, we fabricate PSCs that resemble corten steel and white marble as examples for devices with more demanding aesthetics suited for BIPV (Figure 5b). For the corten steel pattern, a white interlayer of 60% saturation has been incorporated, while no such interlayer is needed for a convincingly looking marble pattern. PSCs with corten steel and white marble pattern yield a PCE up to 7.1% and 14.0%—and on average 38% and 75% relative PCE compared to uncolored reference devices—respectively.

To demonstrate the scalability of the proposed colorization of perovskite photovoltaics, we fabricated a colored small perovskite solar module (PSM) of 9 cm² total area with five interconnected PSCs and 4 cm² active area. As a prominent example of a widely used building material fulfilling customers' high aesthetic demands, a white marble pattern is chosen as a colorization scheme for the PSMs. Since the spin-coated architectures are not suited for upscaling an all-evaporated pin-layer stack as presented in Ritzer et al.^[41] is chosen (see Experimental Section). The PSM in white marble optic displays remarkably high absolute PCE up to 13.9%, which is 88.5% of the average of uncolored reference devices (15.7%). Thereby, our prototype highlights that a high aesthetic value does not necessarily go hand in hand with an immense loss in performance. To the authors' best knowledge, this is the first report on colorful perovskite photovoltaics with a controlled heterochromic pattern. As the PSM's optic is an imitation of traditional building material, these results nourish the hope that customized perovskite photovoltaics will be a publicly accepted and economically viable alternative for such building materials.

5. Conclusion

This work presents an approach for the colorization of perovskite photovoltaics based on inkjet-printed reflective pigments at the front side of perovskite solar modules/cells. To compensate for the dark color of the perovskite absorber, a reflective white interlayer is applied. Via the saturation of this interlayer, the color hue and brightness of the device can be varied and the choice of the ratio of basic printing pigment-inks opens up access to a large variation of colors. Bright mono-colored cyan, magenta, yellow, blue, red, green, and blue PSCs are demonstrated with 70% relative and 12% absolute PCE. Since the color impression is not reliant on interference effects between layers, but generated by selective light reflection of pigment-particles, the color perception is angle-invariant, distinguishing this work from the majority of strategies for colored perovskite photovoltaics. By utilization of the inkjet printing technology, highly adjustable and scalable heterochromic patterns can be printed on the basis of a digital template. As proof of concept, a 9 cm² module (4 cm² active area) in white marble optics with remarkably high PCE of

almost 14%, and 88.5% relative PCE compared to uncolored reference devices is presented. This vivid, angle-invariant, and customizable colorization method may be applicable, where there is a high demand on the aesthetics of the solar cell, opening up future fields of application for colored perovskite photovoltaics in BIPVs.

6. Experimental Section

Colored Glass Substrates: Colored layers were inkjet-printed on the backside of ITO glass substrates with 140 nm thick ITO coating (sheet resistance 15 Ω □⁻², Luminescence Technology, CAS: 50 926-11-9). For this, a modified Roland multipass inkjet printer using five print-heads were used. The 1.6 m × 3 m = 4.8 m² sizing large-area printing table would allow for efficient upscaling. Commercially available inks based on cyan, magenta, yellow, white, and black pigments were deposited via separate parallel mounted overlapping print-heads, allowing for simultaneous multichannel printing of these basic colors. This enabled the printing of mixed homogeneous colors as well as heterogenic color patterns. The colored inks can be printed with varying saturations defined by printer-software-specific parameters, which allow printing layers of controlled thickness. A saturation of 100% equalled a thickness of circa 1.4/3.6/3.0/2.2 μm for white/cyan/magenta/yellow layers. The maximum theoretical printing resolution equals 1480 dpi, which is practically never in use as large format printing does not require fine detailed printing. The multipass printing technology with intermittent integrated drying steps provides separate or slightly overlapping color droplets beside each other rather than a wet-on-wet mixture of colors on the substrate. Printing is done in ambient conditions which might lead to small impurities on a micrometer scale (compare Figure S13 in the Supporting Information). After ink deposition, the colored substrates were annealed at 180 °C for 30 min.

Solar Cells (nip): The devices were fabricated in planar device architecture: glass/ITO/SnO₂/FA_{0.83}Cs_{0.17}Pb_{1.75}Br_{0.25}/spiro-OMeTAD/Au. The above-mentioned uncolored and colored were cleaned 10 min in an ultrasonic bath with deionized (DI) water, acetone, and isopropanol followed by 3 min of oxygen plasma treatment. A thin (≈20 nm) SnO₂ as an electron transport layer was deposited on the ITO substrate by spin coating (4000 rpm for 30 s), followed by an annealing step at 250 °C for 30 min and oxygen plasma treatment for 1 min. The SnO₂ precursor solution was prepared by diluting a 15 wt% aqueous colloidal dispersion of SnO₂ nanoparticles (Alfa Aesar) in DI water to a concentration of 2.5 wt%. The perovskite precursor solution was prepared by dissolving 0.83 mmol formamidinium iodide (Dynamo), 0.17 mmol CsI (abcr), 0.87 mmol PbI₂ (TCI), and 0.13 mmol PbBr₂ (TCI) in a 1 mL solvent mixture of N,N-dimethylformamide (Sigma Aldrich):dimethylsulfoxide (Sigma Aldrich) 4:1 (v:v). The double-cation perovskite absorber layer was deposited on top of the SnO₂ layer from the solution using a two-step spin coating process: 1) 1000 rpm for 10 s; and 2) 5000 rpm for 30 s. Chlorobenzene (150 μL, Sigma Aldrich, CAS: 108-90-7) was poured on the spinning substrate 10 s before the end of the second step. The samples were annealed at 100 °C for 30 min in an inert atmosphere. As an HTL, N²,N²,N²,N²,N⁷,N⁷,N⁷-octakis(4-Methoxyphenyl)-9,9'-Spirobis[9H-Fluoren]-2,2',7,7'-Tetramin (spiro-OMeTAD) was deposited by spin coating (4000 rpm for 30 s). The corresponding precursor solution contained 80 mg spiro-OMeTAD (Luminescence Technology) dissolved in 1 mL chlorobenzene with the additives 17.5 μL lithium bis(trifluoromethanesulfonyl) imide (520 mg mL⁻¹ in acetonitrile) and 4-tert-butylpyridine (28.5 μL). The samples coated with spiro-OMeTAD were exposed to dry air for ≈12 h before a 75 nm thick Au electrode was deposited by thermal evaporation through shadow masks to define the active area to 0.105 cm².

Solar Cells (pin): The devices were fabricated in planar device architecture: glass/ITO/2PACz/FA_{0.82}Cs_{0.18} PbI₃/C₆₀/BCP/Ag. The above-mentioned uncolored and colored were cleaned 10 min in an ultrasonic bath with DI water, acetone, and isopropanol followed by 3 min of oxygen plasma treatment. A thin 2PACz HTL was deposited on the ITO substrate by spin-coating at 3000 rpm for 30 s, followed by an annealing step at

100 °C for 10 min. The 2PACz precursor solution was prepared by dissolving 2 PACz powder in anhydrous ethanol at a concentration of 1 mmol/l and put into an ultrasonic bath for 15 min before use. The perovskite precursor solution was prepared by dissolving 0.82 mmol formamidinium iodide (Dynamo), 0.18 mmol CsCl (abcr), 1.1 mmol PbI₂ (TCI), in a 1 mL solvent mixture of *N,N*-dimethylformamide (Sigma Aldrich):dimethylsulfoxide (Sigma Aldrich) 4:1 (v:v). 35 μ L of PbCl₂:MAcI solution with a molar ratio of 1:1 dissolved in 1 mL DMSO was added as an additive in the reference perovskite precursor solution. The double-cation perovskite absorber layer was deposited on top of 2PACz from solution using a two-step spin coating process: 1) 1000 rpm for 10 s; and 2) 5000 rpm for 30 s. Chlorobenzene (150 μ L, Sigma Aldrich, CAS: 108-90-7) was poured on the spinning substrate 10 s before the end of the second step. The samples were annealed at 150 °C for 30 min in an inert nitrogen atmosphere. After perovskite annealing, 1 nm lithium fluoride (LiF), 23 nm C₆₀ (Sigma), and 8 nm bathocuproine (BCP, Luminescence Technology) were thermally evaporated with an evaporation rate of 0.1–2 Å s^{-1} at a pressure of 10^{−6} mbar. Afterward, a 100 nm thick Ag electrode was deposited by thermal evaporation through shadow masks to define the active area to 0.105 cm².

Solar Modules: The employed layer stack sequence ITO/spiro-TTB/MAPI/C₆₀/BCP/Au for the all-evaporated solar cells and modules was discussed in detail in a previous publication.^[41] Glass substrates (9 cm² substrate size) coated with unpatterned ITO, Luminescence Technology, CAS: 50926-11-9, were laser-scribed to obtain the transparent electrode structure. Deposition of color was done as described previously. The substrates were cleaned in acetone and isopropanol in an ultrasonic bath for 10 min each before deposition of the color. Immediately before the deposition of the charge transport layers, they were bathed in isopropanol for 2 min followed by an additional cleaning step in an oxygen plasma for 3 min. Afterward, the substrates were transferred into a nitrogen-filled glovebox for the deposition of the functional layers and not exposed to air anymore. The <5 nm thick 2,2',7,7'-tetra(*N,N*-di-*p*-tolyl) amino-9,9-spirobifluorene (spiro-TTB, Luminescence Technology, CAS: 515834-67-0) was thermally evaporated in an OPTIvap evaporation system (CreaPhys GmbH) without any doping. The perovskite absorber was fabricated by co-evaporation of lead iodide (PbI₂, TCI Deutschland GmbH, 99.99% purity, CAS: 10101-63-0) and methylammonium iodide (CH₃NH₃I, Luminescence Technology, >99.5% purity, CAS: 14965-49-2) in a PEROvap evaporations system (CreaPhys GmbH). PbI₂ was used for several consecutive evaporation runs while CH₃NH₃I was replaced after every deposition. Substrates and materials were kept in high vacuum for outgassing before deposition overnight. To prevent a strong rise in CH₃NH₃I background pressure and to facilitate rate detection, the evaporation system was equipped with cooling shields around the evaporation sources cooled down to a temperature below −15 °C. PbI₂ was evaporated at an evaporation rate of 1.5 Å s^{-1} , CH₃NH₃I at an evaporation rate between 2.0 and 2.5 Å s^{-1} . Substrates were kept at a temperature of 25 °C during deposition. After deposition of the absorber, samples were transferred back to the previous evaporation system for the deposition of a 25 nm thick C60 fullerene layer (Alfa Aesar, 98%, CAS: 99 685-96-8) and a 6 nm thick BCP layer. Finally, a 100 nm thick gold contact was deposited. A laser-scribing process was used to give an active device area of five interconnected solar cells with an active area of 0.8 cm² each, resulting in a solar module with a 4 cm² aperture size.

Color Characterization: Color impression was characterized by an x-rite SpectroEye spectral photometer. The samples were illuminated by a built-in light source and the reemission was measured by the built-in photodetector. In conformance to global industry standards, a CIE Standard Illuminant D65 (mathematical representation of noon skylight, color temperature 6500 K) was chosen.^[42,43] Measurements were taken and presented in the CIELAB-color space (also CIE L* a* b*) where the three coordinates represent the lightness of the color (L*), its position between red and green (a*), and its position between yellow and blue (b*).^[42,44] For presentation, measurements were additionally converted to CIE 1931- and RGB-color spaces.^[42,44]

UV–Vis–NIR-Transmittance Measurements: Transmittance and reflectivity were measured with a spectrophotometer (Perkin Elmer Lambda 1050) with an integrating sphere.

Angle-Dependent Color Characterization: For angle-dependent color characterization, a Konica Minolta Chroma-Meter CS-200 luminance and chromaticity measurement camera was used. The viewing angle was varied by adjustment of the camera in angle, height, and distance, so that the light path from the sample to the camera is unchanged. Samples were illuminated by homogeneous but not standardized room light (halogen lamp) for all angles. Measurements were taken in the CIE 1931-color space and additionally converted to the CIELAB color space.^[42,44] Due to the utilization of a non-standardized illuminator, a small shift in the overall measured color coordinates could be observed for the 0° observation angle compared to the measurements with the CIE Standard Illuminant D65. This was addressed by normalization of all color values according to the shift at 0°.

Solar Cell Characteristics: Standardly, for measurements of the solar cell characteristics, a class AAA xenon-lamp-based solar simulator (Newport Oriel Sol3A) was used (compare Figure S14, Supporting Information, for details on the spectrum). To estimate the effect of repeated light reflection between (colored) the front side of the substrate and the solar simulator setup (lenses/mirror), a class AAA 21-channel LED solar simulator (Wavelabs Solar Metrology Systems Sinus-70) was used for reference measurements. Both solar simulators are located inside a nitrogen-filled glovebox. The AM1.5G spectrum (100 mW cm^{−2}) was calibrated with a KG5 band pass-filtered n-silicon reference solar cell (Newport Oriel, calibrated and certified on July 31, 2019). The cells were then measured in both backward and forward direction with a constant scan rate of circa 0.6 V s^{−1} (Keithley 2400 source measurement unit) while holding the temperature of the solar cell at 25 °C with a microcontroller-adjusted Peltier-element. The entire device area was illuminated with the active area defined by the electrode layout. Measurements were done without any pre-conditioning prior to measurements. Spectral mismatch between reference cells and testing cells is limited to 4% (and 0.7%, respectively) for the solar simulators.

EQE Measurements: EQE measurements were performed using a Bentham EQE system. A chopping frequency of \approx 930 Hz with an integration time of 500 ms was used to obtain the spectra. An adjustable substrate table was used to vary the angle of the substrate's surface relatively to the excitation light source.

Supporting Information

Supporting Information is available from the Wiley Online Library or from the author.

Acknowledgements

All authors contributed equally to this work. The financial support by the Federal Ministry for Research and Education (BMBF) through the project PRINTPERO (03SF0557A), the Funding of the Helmholtz Association (HYIG of U.W.P. (VH-NG-1148)); Recruitment Initiative of B.S.R.; the Helmholtz Energy Materials Foundry (HEMF); PEROSEED (ZT-0024); and the Karlsruhe School of Optics & Photonics (KSOP) is gratefully acknowledged. The authors received further support from the Helmholtz Association Program: Program oriented funding IV, Materials and Technologies for the Energy Transition, Topic 1: Photovoltaics and Wind Energy, Code: 38.01.04. The authors would like to thank the members of the Perovskite Taskforce at Light Technology Institute and the Institute of Microstructure Technology as well as the Printed Electronics research group at InnovationLab Heidelberg for support in our scientific work, especially to Ahmed Farag for supporting SEM measurements.

Open access funding enabled and organized by Projekt DEAL.

Conflict of Interest

The authors declare no conflict of interest.

Data Availability Statement

The data that support the findings of this study are available from the corresponding author upon reasonable request.

Keywords

building-integrated photovoltaics, colors, inkjet printing, perovskite solar cells

Received: October 27, 2021

Revised: December 12, 2021

Published online: January 27, 2022

- [1] A. Henemann, *Renewable Energy Focus* **2008**, *9*, 14.
- [2] C. Ballif, L. E. Perret-Aebi, S. Lufkin, E. Rey, *Nat. Energy* **2018**, *3*, 438.
- [3] NREL, Best Research-Cell Efficiency Chart, can be found under <https://www.nrel.gov/pv/cell-efficiency.html> (accessed: January 2022).
- [4] Y. Peng, F. Zeng, Y. Cheng, C. Wang, K. Huang, P. Xie, H. Xie, Y. Gao, J. Yang, *Org. Electron.* **2020**, *83*, 105736.
- [5] W. Wu, P. N. Rudd, Q. Wang, Z. Yang, J. Huang, *Adv. Mater.* **2020**, *32*, 2000995.
- [6] H. Eggers, F. Schackmar, T. Abzieher, Q. Sun, U. Lemmer, Y. Vaynzof, B. S. Richards, G. Hernandez-Sosa, U. W. Paetzold, *Adv. Energy Mater.* **2020**, *10*, 2000271 <https://doi.org/10.1002/aenm.201903184>.
- [7] F. Schackmar, H. Eggers, M. Frericks, B. S. Richards, U. Lemmer, G. Hernandez-Sosa, U. W. Paetzold, *Adv. Mater. Technol.* **2021**, *6*, 2000271 <https://doi.org/10.1002/admt.202000271>.
- [8] Y. Vaynzof, *Adv. Energy Mater.* **2020**, *10*, 2003073.
- [9] T. Abzieher, T. Feeney, F. Schackmar, Y. J. Donie, I. M. Hossain, J. A. Schwenzler, T. Hellmann, T. Mayer, M. Powalla, U. W. Paetzold, *Adv. Funct. Mater.* **2021**, *31*, 2104482.
- [10] Q. Xue, R. Xia, C. J. Brabec, H. L. Yip, *Energy Environ. Sci.* **2018**, *11*, 1688.
- [11] S. Rahmany, L. Etgar, *ACS Energy Lett.* **2020**, *5*, 1519.
- [12] D. E. Attoye, K. A. T. Aoul, A. Hassan, *Sustainability* **2017**, *9*, 2287.
- [13] A. Prieto, U. Knaack, T. Auer, T. Klein, *J. Facade Des. Eng.* **2017**, *5*, 51.
- [14] T. E. Kuhn, C. Erban, M. Heinrich, J. Eisenlohr, F. Ensslen, D. H. Neuhaus, *Energy Build.* **2021**, *231*, 110381.
- [15] C. Erban, H. Ley, in *EUPVSEC Conf. Proc. 2020*, Lissabon **2020**, pp. 2063–2067 <https://www.eupvsec-proceedings.com/proceedings?paper=48854>.
- [16] R. J. Yang, P. X. W. Zou, *Int. J. Construct. Manage.* **2016**, *16*, 39.
- [17] G. P. Hammond, H. A. Harajli, C. I. Jones, A. B. Winnett, *Energy Policy* **2012**, *40*, 219.
- [18] J. Koinegg, T. Brudermann, A. Posch, M. Mrotzek, *GAIA* **2013**, *22*, 39.
- [19] K. T. Lee, M. Fukuda, S. Joglekar, L. J. Guo, *J. Mater. Chem. C* **2015**, *3*, 5377.
- [20] J. W. Jung, C.-C. Chueh, A. K.-Y. Jen, *Adv. Energy Mater.* **2015**, *5*, 1500486.
- [21] G. E. Eperon, D. Bryant, J. Troughton, S. D. Stranks, M. B. Johnston, T. Watson, D. A. Worsley, H. J. Snaith, *J. Phys. Chem. Lett.* **2015**, *6*, 129.
- [22] J. H. Lu, Y. L. Yu, S. R. Chuang, C. H. Yeh, C. P. Chen, *J. Phys. Chem. C* **2016**, *120*, 4233.
- [23] C. O. Ramírez Quiroz, C. Bronnbauer, I. Levchuk, Y. Hou, C. J. Brabec, K. Forberich, *ACS Nano* **2016**, *10*, 5104.
- [24] K. T. Lee, J. Y. Jang, S. J. Park, S. A. Ok, H. J. Park, *Nanoscale* **2017**, *9*, 13983.
- [25] K. T. Lee, J. Y. Jang, N. Y. Ha, S. Lee, H. J. Park, *Nano Res.* **2018**, *11*, 2553.
- [26] M. B. Upama, M. A. Mahmud, H. Yi, N. K. Elumalai, G. Conibeer, D. Wang, C. Xu, A. Uddin, *Org. Electron.* **2019**, *65*, 401.
- [27] Y. Deng, Q. Wang, Y. Yuan, J. Huang, *Mater. Horizons* **2015**, *2*, 578.
- [28] W. Zhang, M. Anaya, G. Lozano, M. E. Calvo, M. B. Johnston, H. Míguez, H. J. Snaith, *Nano Lett.* **2015**, *15*, 1698.
- [29] Y. Jiang, B. Luo, F. Jiang, F. Jiang, C. Fuentes-Hernandez, T. Liu, L. Mao, S. Xiong, Z. Li, T. Wang, B. Kippelen, Y. Zhou, *Nano Lett.* **2016**, *16*, 7829.
- [30] D. Cui, Z. Yang, D. Yang, X. Ren, Y. Liu, Q. Wei, H. Fan, J. Zeng, S. Liu, *J. Phys. Chem. C* **2016**, *120*, 42.
- [31] K. T. Lee, J. Y. Jang, J. Zhang, S. M. Yang, S. Park, H. J. Park, *Sci. Rep.* **2017**, *7*, 10640 <https://doi.org/10.1038/s41598-017-10937-3>.
- [32] S. Schliske, F. Mathies, D. Busko, N. Strobel, T. Rödlmeier, B. S. Richards, U. Lemmer, U. W. Paetzold, G. Hernandez-Sosa, E. Klampafitis, *ACS Appl. Energy Mater.* **2019**, *2*, 764.
- [33] H. Wang, H. A. Dewi, T. M. Koh, A. Bruno, S. Mhaisalkar, N. Mathews, *ACS Appl. Mater. Interfaces* **2020**, *12*, 484.
- [34] G. Y. Yoo, R. Azmi, C. Kim, W. Kim, B. K. Min, S. Y. Jang, Y. R. Do, *ACS Nano* **2019**, *13*, 10129.
- [35] J. H. Noh, S. H. Im, J. H. Heo, T. N. Mandal, S. Il Seok, *Nano Lett.* **2013**, *13*, 1764.
- [36] H. Lee, H. J. Song, *WIREs Energy Environ* **2021**, *10*, e403 <https://doi.org/10.1002/wene.403>.
- [37] J. Halme, P. Mäkinen, *Energy Environ. Sci.* **2019**, *12*, 1274.
- [38] BIPV Hersteller - SUNOVATION | Building Integrated Photovoltaics, can be found under <https://sunovation.de/de/> (accessed: November 2021).
- [39] F. Corsini, G. Griffini, *J. Phys. Energy* **2020**, *2*, 031002.
- [40] B. Bläsi, T. Kroyer, T. Kuhn, O. Hohn, *IEEE J. Photovoltaics* **2021**, *11*, 1305.
- [41] D. B. Ritzer, T. Abzieher, A. Basibüyük, T. Feeney, F. Laufer, S. Ternes, B. S. Richards, S. Bergfeld, U. W. Paetzold, *Prog. Photovoltaics Res. Appl.* **2021**, *1* <https://doi.org/10.1002/pip.3489>.
- [42] CIE, *CIE 015:2018 Colorimetry*, International Commission of Illumination 4th ed., **2018**, ISO 11664-2:2007(E)/CIE S 014-2/E:2006 <https://cie.co.at/publications>.
- [43] CIE, *CIE ISO DIS 11664-2:2020 Colorimetry - Part 2: CIE Standard Illuminants*, **2020**.
- [44] CIE, *ISO/CIE 11664-4:2019 Colorimetry - Part 4: CIE 1976 L*a*b* Colour Space*, International Commission of Illumination **2019** <https://cie.co.at/publications>.